

# Prereduction of Metal Oxides via Carbon Plasma Treatment for Efficient and Stable Electrocatalytic Hydrogen Evolution

Yongqi Zhang, Bo Ouyang, Kun Xu, Xinhui Xia, Zheng Zhang, Rajdeep Singh Rawat, and Hong Jin Fan\*

**Prereduction of transition metal oxides is a feasible and efficient strategy to enhance their catalytic activity for hydrogen evolution. Unfortunately, the prereduction via the common H<sub>2</sub> annealing method is unstable for nanomaterials during the hydrogen evolution process. Here, using NiMoO<sub>4</sub> nanowire arrays as the example, it is demonstrated that carbon plasma (C-plasma) treatment can greatly enhance both the catalytic activity and the long-term stability of transition metal oxides for hydrogen evolution. The C-plasma treatment has two functions at the same time: it induces partial surface reduction of the NiMoO<sub>4</sub> nanowire to form Ni<sub>4</sub>Mo nanoclusters, and simultaneously deposits a thin graphitic carbon shell. As a result, the C-plasma treated NiMoO<sub>4</sub> can maintain its array morphology, chemical composition, and catalytic activity during long-term intermittent hydrogen evolution process. This work may pave a new way for simultaneous activation and stabilization of transition metal oxide-based electrocatalysts.**

Hydrogen evolution from water splitting offers a sustainable method to acquire molecular hydrogen (H<sub>2</sub>) fuel, an ideal alternative to fossil fuels without CO<sub>2</sub> emission.<sup>[1–4]</sup> To make this technology viable, the catalyst in an electrolysis device should exhibit both high electrocatalytic activity and long-term durability. In this regard, catalysts based on precious metals, such as Pt, meet the above-mentioned characteristics, but their scarcity, high cost and poor stability are hindrance to any large-scale

industrial H<sub>2</sub> production.<sup>[5–7]</sup> Therefore, the realization of hydrogen economy relies largely on the development of high-efficiency, cost-effective and durable alternatives as hydrogen evolution reaction (HER) electrocatalysts.

In the past few decades, intensive research efforts have been focused on transition metal-based materials, such as nitrides,<sup>[8,9]</sup> carbides,<sup>[10,11]</sup> sulfides,<sup>[12–14]</sup> phosphides,<sup>[15–17]</sup> as efficient candidates for HER catalysts due to their low cost, earth abundance, and optimal strength of metal hydride bond (M-H). Nevertheless, most of the above catalysts are fabricated from high-temperature annealing in harsh environments that involve poisonous feedstock and byproduct. Even worse, the indispensable high temperature annealing

process makes it nearly impossible to maintain the high-specific-area nanostructures, which is important for an efficient catalyst. By contrast, transitional metal oxides are easily available compound materials with a wide variety of nanostructures with high specific surface area.<sup>[18]</sup> However, most of them fail to play an important role in hydrogen evolution due to their low electrical conductivity, sluggish catalytic kinetics, and poor long-term stability. In this regard, it is highly desirable to improve the HER performance of transition metal oxides.


Recently, there has been a few reports that modulation of the local atomic structure via introducing oxygen vacancy could improve the HER activity for certain metal oxides.<sup>[19,20]</sup> For example, Yang and co-workers reported that the commercial WO<sub>3</sub> nanoparticles can show enhanced HER activity after annealing under H<sub>2</sub> atmosphere.<sup>[20]</sup> In addition, we found that metal oxides (herein, NiMoO<sub>4</sub>, Co<sub>3</sub>O<sub>4</sub>, and NiO) show a self-activation effect during the continuous hydrogen evolution process (Figure S1, Supporting Information). The activity improvement is probably due to the surface reduction of metal oxides by the highly active hydrogen atoms that are produced on their surface during the HER process. This phenomenon is similar to the surface oxidation of some nonoxide catalysts during oxygen evolution reaction process.<sup>[21,22]</sup> However, this in situ improvement by self-activation is slow (takes a few hours), transient, and extremely unstable; the catalytic activity degrades quickly when the H<sub>2</sub> evolution is interrupted (Figure S1d, Supporting Information). So prereduction of metal oxides should be a more feasible and efficient strategy to improve their HER catalytic activity. H<sub>2</sub> annealing is a commonly employed for

Y. Q. Zhang, Dr. K. Xu, Prof. H. J. Fan  
School of Physical and Mathematical Sciences  
Nanyang Technological University  
637371, Singapore  
E-mail: fanhj@ntu.edu.sg

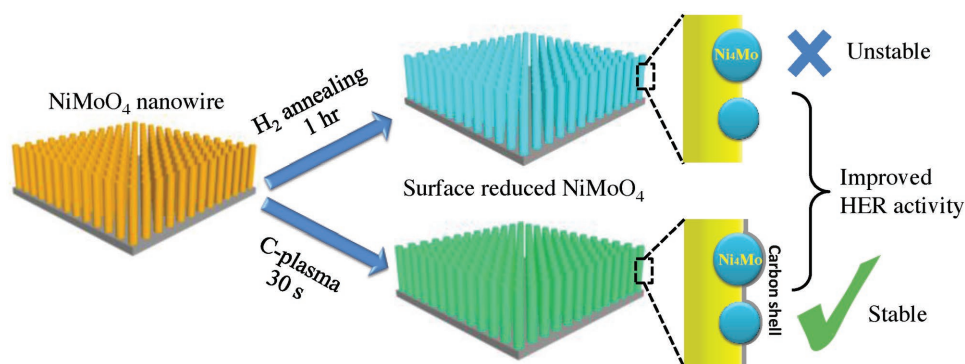
B. Ouyang, Prof. R. S. Rawat  
Natural Sciences and Science Education  
National Institute of Education  
Nanyang Technological University  
637616, Singapore

Prof. X. Xia  
State Key Laboratory of Silicon Materials and Department  
of Materials Science and Engineering  
Zhejiang University  
Hangzhou 310027, P. R. China

Dr. Z. Zhang  
Institute of Materials Research and Engineering  
A\*STAR (Agency for Science, Technology and Research)  
#08-03, 2 Fusionopolis Way, Innovis 138634, Singapore

 The ORCID identification number(s) for the author(s) of this article can be found under <https://doi.org/10.1002/smll.201800340>.

DOI: 10.1002/smll.201800340



**Scheme 1.** The preparation of C-plasma treated and H<sub>2</sub> annealed NiMoO<sub>4</sub>.

prereduction of metal oxides. Unfortunately, the high temperature and long annealing time may destroy the nanostructure. Also the reduction is still unstable and obvious degradation of HER catalytic activity is observed for the H<sub>2</sub>-annealed NiMoO<sub>4</sub>, Co<sub>3</sub>O<sub>4</sub>, and NiO (see Figure S1d, Supporting Information). Zhang et al.<sup>[23]</sup> and Chen et al.<sup>[24]</sup> treated NiMoO<sub>4</sub> nanorods by reducing under an H<sub>2</sub> atmosphere. While the electrodes after H<sub>2</sub> reduction show good catalytic performance in both studies, the nanorod surfaces were directly exposed and might be subject to oxidation during operation in the KOH electrolyte. This has been demonstrated in our experiment (Figure S1d, Supporting Information). Therefore, it becomes necessary that a surface modification to the transition metal oxides should simultaneously improve the catalytic activity and stability, and maintain the nanostructures.

Herein, we report a more efficient method to boost the HER catalytic activity of metal oxides with more stable performance via carbon plasma modification. Plasma treatment has been reported recently as a powerful approach for surface conversion reaction and modification of the electrode materials.<sup>[25–30]</sup> In this work, we take NiMoO<sub>4</sub> nanowire arrays on carbon cloth as a case study. As shown in the **Scheme 1**, after the C-plasma treatment, active species of Ni<sub>4</sub>Mo nanoparticles are produced due to reduction of the NiMoO<sub>4</sub>. And the nanowire array structure is well preserved due to a very short process time (30 s). In the meantime a thin outer layer of carbon shell is deposited on the nanowire surface, which assures the chemical stability by preventing oxidation. Benefiting from the high exposed surface active sites (nanowire array), the generated active Ni–Mo alloy nanoparticles and the protection of carbon shell, the C-plasma treated NiMoO<sub>4</sub> nanowire electrode displayed a low overpotential of 76 mV to reach 10 mA cm<sup>−2</sup> in 1 M KOH and superior duration in intermittent operation condition. This strategy is generic and also effective for Co<sub>3</sub>O<sub>4</sub> nanowire arrays. Our work offers a feasible plasma-assisted strategy toward activation and stabilization of transition metal oxide-based electrocatalysts.

To prepare the C-plasma treated NiMoO<sub>4</sub> electrocatalyst, the common NiMoO<sub>4</sub> nanowire arrays were fabricated via a solvothermal method. And then the obtained NiMoO<sub>4</sub> was treated under C-plasma atmosphere at different plasma discharge duration: 15, 30, and 60 s, corresponding to the products of C-15s, C-30s, and C-60s, respectively, and presented in Figure S2 of the Supporting Information. **Figure 1** shows the detailed morphological structures of the C-30s. The

morphology of nanowire arrays was preserved and many nanoparticles with the diameter of 5–10 nm were separated out on the surface of nanowires (Figure 1a,b). In the high magnified transmission electron microscopy (TEM) images (Figure 1c,d), *d*-spacing of 0.208 and 0.180 nm were measured for the nanoparticles, which corresponds to the (121) and (310) plane of the Ni<sub>4</sub>Mo alloy (PDF# 65–5480). This indicates that Ni<sub>4</sub>Mo alloy could be separated under the reductive atmosphere, which is in agreement with previous reports.<sup>[23,31]</sup> About 1–2 layers of carbon were coated on the surface of nanowire. By their nature of catalytic decomposition of ethanol, Ni<sub>4</sub>Mo nanoparticles have a thicker carbon shell, which is around 2 nm, corresponding to four graphitic layers. Furthermore, a high-angle annular dark-field scanning transmission electron microscopy (STEM) image further confirmed that the metal nanoparticles decorated nanowires were formed (Figure 1e). As presented in the corresponding energy-dispersive X-ray (EDX) mappings, the Mo, O, and C elements were homogeneously distributed throughout the whole nanowire, while the Ni element was distributed granularly on the surface with distinguishable particle boundaries. The STEM-EDX line analysis of the C-30s along the noted path in Figure S3 of the Supporting Information further reveals the enrichment of Ni element. The energy dispersive spectroscopy confirms that the molar ratio of Ni to Mo is ≈1.05:1 (Figure S3c, Supporting Information). The X-ray diffraction (XRD) patterns in Figure S4 of the Supporting Information confirm that NiMoO<sub>4</sub> was converted into Ni<sub>4</sub>Mo and MoO<sub>2</sub> after 30 s C-plasma treatment.

The surface chemical composition and valence states of samples were further characterized by X-ray photoelectron spectroscopy (XPS; **Figure 2**; Figure S5, Supporting Information). Four elements including Ni, Mo, O, and C were identified from the XPS spectra (Figure S5a, Supporting Information), consistent with EDX mapping results. With the increasing treatment duration, the peak intensities of Ni, Mo, and O became weaker, while the peak intensities of C became stronger. For C-60s, the layer of carbon was too thick to detect the signal of Ni, Mo, and O. For the high resolution spectra of Ni 2p (Figure 2a), the peak at 855.6 eV and its broad satellite peak at 861.8 eV belongs to Ni<sup>2+</sup>. After 30 s C-plasma treatment, the new peak at 852.4 eV is indexed to metallic Ni.<sup>[32]</sup> The partial reduction of NiMoO<sub>4</sub> under C-plasma treatment could also be seen from the O 1s spectra (Figure 2b). As exhibited, the intensity of the peak at 530.7 eV, corresponding to the O<sup>2−</sup> ions in the crystal line of

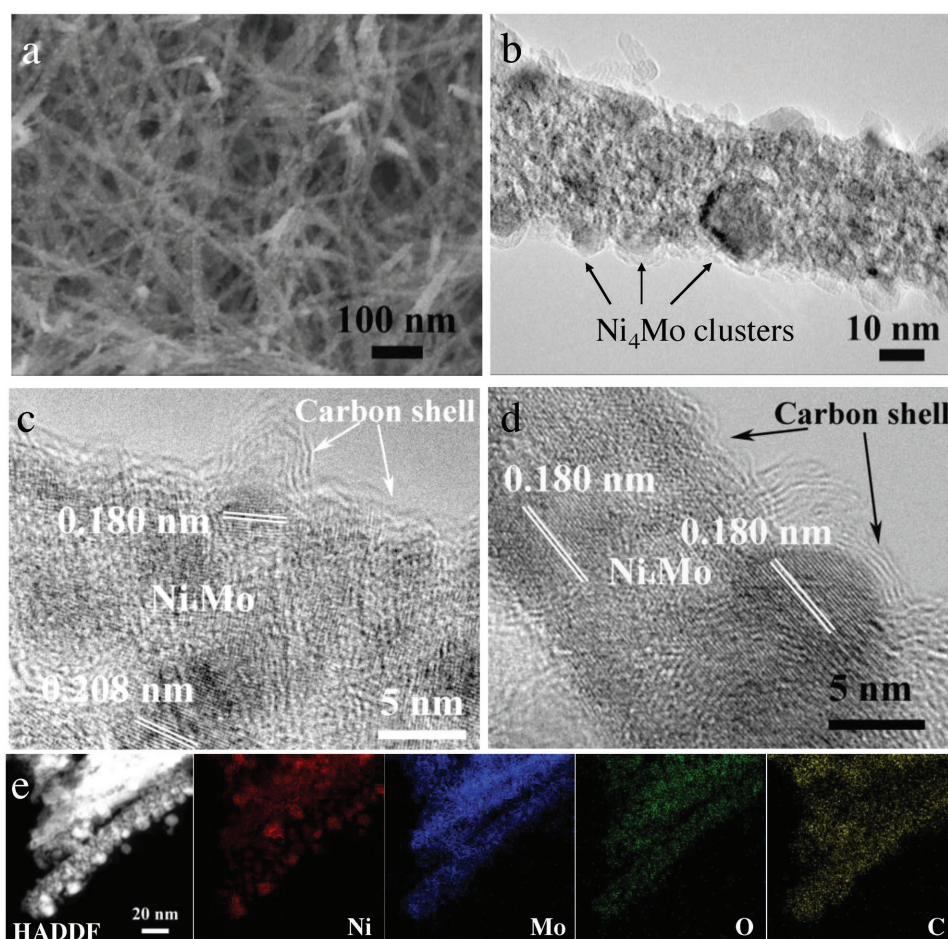


**Figure 1.** Electron microscopy images of C-30s: a) SEM, b–d) TEM, and e) STEM image and EDX elemental mapping.

NiMoO<sub>4</sub>, decreased for the C-30s sample.<sup>[21]</sup> A new peak from the surface groups of carbon shell appeared at 531.8 eV. The Mo 3d spectra in Figure 2c displays a new peak at low binding energy at 229.4 eV after C-plasma treatment, which attributes to low valence Mo<sup>δ+</sup> species ( $\delta = 0, 1, 2, 3$ ).<sup>[33]</sup> The percentage of Mo<sup>δ+</sup> in C-30s is 40.2%, which is higher than that of C-15s (12.7%) as compared in Table S1 (Figure S5b, Supporting Information). The ratio of Ni:Mo is around 1.1:1 based on the XPS spectra of Ni 2p and Mo 3d. The slight higher ratio of Ni element is probably due to the enrichment of Ni on the surface. The C 1s spectra in Figure 2d only manifest the graphitic carbon at 284.3 eV, and no carbide peak (lower binding energy,  $\approx 282.7$  eV) was observed.

The electrocatalytic activity of all samples for HER were evaluated by a three-electrode system in 1 M KOH (Figure 3) and compared to the state-of-the-art Pt/C electrocatalysts. Carbon rod was used as the counter electrode to avoid the possible contamination of Pt. The polarization curves at a sweep rate of 5 mV s<sup>-1</sup> after iR-correction show an increase in the HER activity in the following order: NiMoO<sub>4</sub>, C-15s, C-60s, C-30s, and Pt/C. The overpotential of only 76 mV is required for C-30s sample to reach a current density of 10 mA cm<sup>-2</sup> ( $\eta_{10}$ ), which is slightly higher than that of Pt/C (45 mV) and obviously lower than that of NiMoO<sub>4</sub> (406 mV), C-15s (135 mV), and C-60s (152 mV).

The inferior HER activity of C-60s attributes to the thicker and hollow carbon shell, which blocks the active sites from electrolyte. In addition, the overpotential of C-30s is only 287 mV to reach a high current density of 300 mA cm<sup>-2</sup> (Figure S6, Supporting Information). The Tafel slope, as one of the experimental descriptor to study the HER kinetics, were obtained by plotting the overpotential versus the logarithm of the absolute value of current density (Figure 3b). The Tafel slope of C-30s (78 mV dec<sup>-1</sup>) is smaller than those of NiMoO<sub>4</sub> (130 mV dec<sup>-1</sup>), C-15s (106 mV dec<sup>-1</sup>), and C-60s (103 mV dec<sup>-1</sup>). The comparison of Tafel slope versus  $\eta_{10}$  value for all of the studied catalysts in Figure 3c has clearly shown that the C-plasma treated NiMoO<sub>4</sub> had significantly improve the HER catalytic activity (larger current density and faster HER rates). The C-30s electrode exhibits comparable HER catalytic activity to those transition metal-based materials reported in the literature (Table S2, Supporting Information). To better understand the superior HER activity of C-plasma treated NiMoO<sub>4</sub>, their electrochemical impedance spectroscopies (EIS) were carried out to study the kinetics occurring at the electrode/electrolyte surface under HER conditions. The typical Nyquist plots in Figure 3d depict the diameter of the semicircles decreased in the following order: NiMoO<sub>4</sub>, C-15s, C-60s, and C-30s, indicating that C-30s has the fastest electron transfer and HER activation.



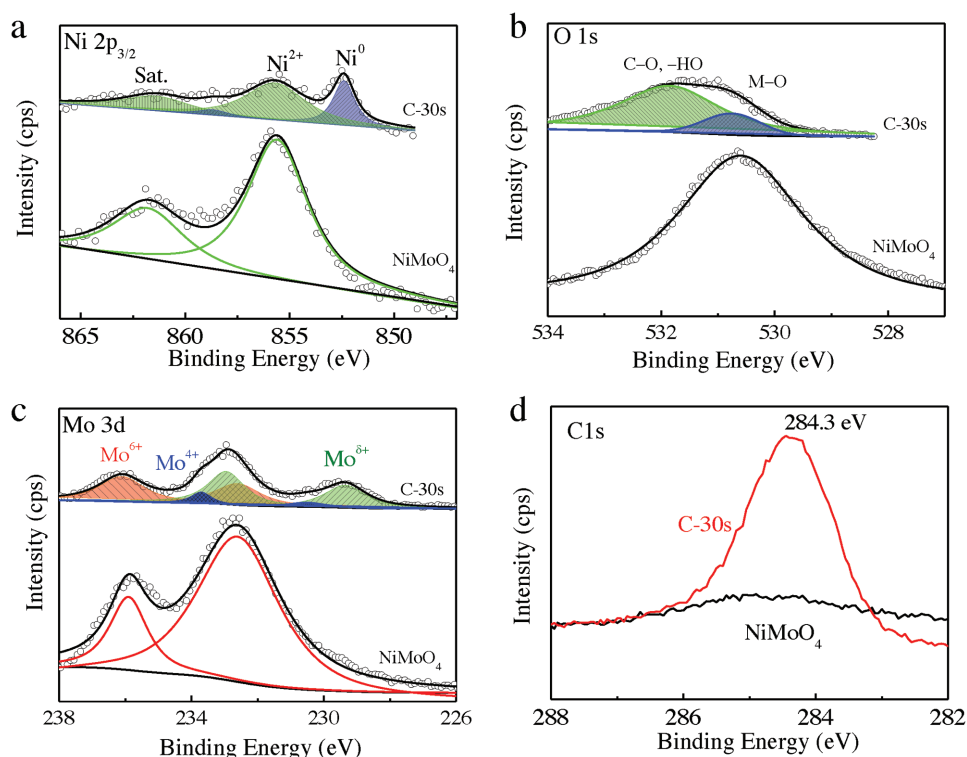


**Figure 2.** High-resolution XPS for NiMoO<sub>4</sub> and C-30s a) Ni 2p<sub>3/2</sub>, b) O 1s, c) Mo 3d, and d) C 1s.

The C-30s sample also exhibits an excellent long-term electrochemical stability. As shown in **Figure 4**, Electrolysis at three constant current densities (10, 30, and 50 mA cm<sup>-2</sup>) was carried out sequentially over 36 h (Figure 4a). The overpotentials at different current densities show a relatively small fluctuation after each 12 h electrolysis (−4, 8, and 17 mV at 10, 30, and 50 mA cm<sup>-2</sup>, respectively). The slight decrease of overpotential at 10 mA cm<sup>-2</sup> was probably due to the penetration of electrolyte to expose more active sites. The degradation at 30 and 50 mA cm<sup>-2</sup> was partially due to reduced active sites caused by the physical adsorption of the generated H<sub>2</sub>. As shown in Figure 4b, the linear sweep voltammetry (LSV) curves after electrolysis at different current densities almost overlap with the original one. In addition, a multistep chronoamperometric curve was recorded in a wide overpotential range (from 50 to 500 mV) with an increment of 50 mV (Figure 4c). The response current densities remain constant at each step, implying the excellent mass transportation, conductivity, and mechanical robustness of the C-30s electrode.

The electrode also maintains its morphology and chemical composition after the 36 h stability test (**Figure 5**). The nanowire array morphology and the layer of carbon shell were well preserved, as shown by scanning electron microscopy (SEM) and TEM images in Figure 5a,b. The Ni<sub>4</sub>Mo nanoparticles are clearly observed in nanowires, owing to the protection provided by the carbon shell. We also compare the XPS spectra of Ni and Mo before and after stability test (Figure 5c,d). The peaks due to both Ni<sup>0</sup> and Mo<sup>δ+</sup> remain except for slight decrease in their intensities. This verifies that the C-30s sample is not only a highly active but also a very stable electrocatalyst for HER in alkaline medium.

In order to verify the contribution of C shell, we intentionally synthesized a hydrogen-reduced NiMoO<sub>4</sub> nanowires film in gas ambient (H<sub>2</sub>-1h) and investigated its catalytic enhancement and stability. Surface treatment of the NiMoO<sub>4</sub> nanowires in an H<sub>2</sub> gas ambient can also improve the catalyst activity, but cannot solve instability problem. The synthetic and structural details of H<sub>2</sub>-1h were presented in the Experimental Section and Figure S7 of the Supporting Information. The SEM image (Figure S7a, Supporting Information) and XRD pattern (Figure S7b, Supporting Information) confirmed that indeed Ni<sub>4</sub>Mo nanoparticles were formed on the surface of nanowires, similar to carbon-plasma reduction. Furthermore, the surface chemical composition and valence states of H<sub>2</sub>-1h were the same as those of C-30s (XPS of Ni and Mo in Figure S8d,e, Supporting Information). A current density of 10 mA cm<sup>-2</sup> was achieved with an overpotential of only 60 mV in 1 M KOH, which was better than that of C-30s (76 mV) (Figure S7c, Supporting Information). However, it is quite unstable. After 1–2 h stability test at 10 mA cm<sup>-2</sup>, the overpotential of H<sub>2</sub>-1h was higher than that of C-30s (Figure 4a). If soaking the H<sub>2</sub>-1h in electrolyte for only 30 min, the  $\eta_{10}$  would sharply increase to ≈223 mV (Figure S7c, Supporting Information). The XPS spectra of Ni and Mo, after the 30 min soaking (Figure S8d,e, Supporting Information), showed that both peaks for Ni<sup>0</sup> and Mo<sup>δ+</sup> disappeared. So the active sites are most likely Ni<sub>4</sub>Mo and low valence (Mo<sup>δ+</sup>).<sup>[34]</sup> To further check their chemical stability, the NiMoO<sub>4</sub>, H<sub>2</sub>-1h, and C-30s samples were immersed in 1 M KOH solution for 12 h (without electrochemical measurement). We found the nanowire arrays of the NiMoO<sub>4</sub> and H<sub>2</sub>-1h samples almost disappeared, but

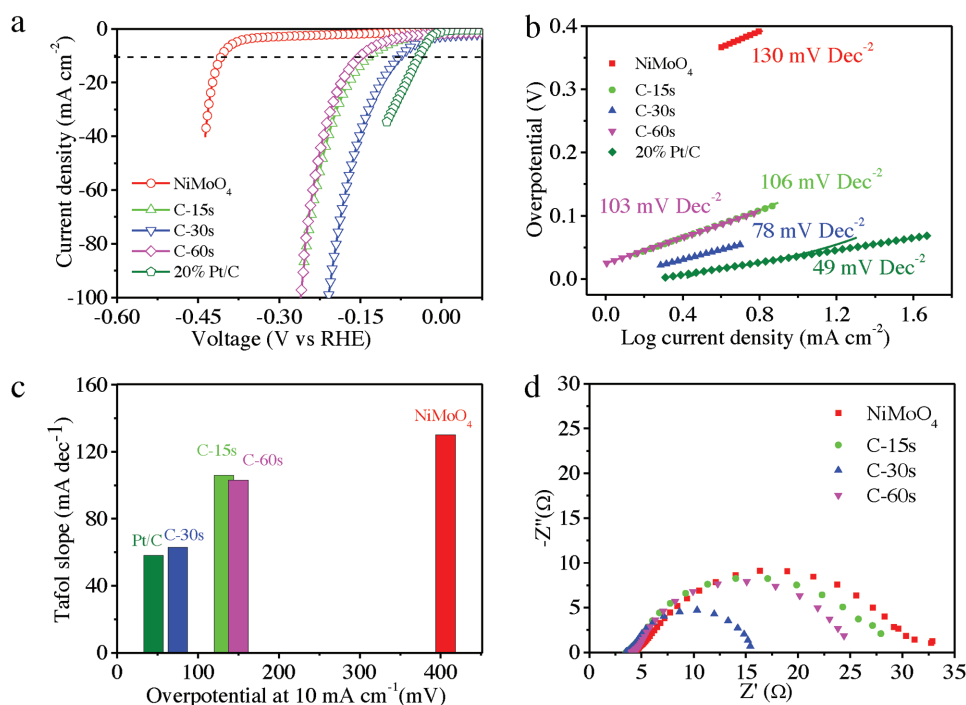


**Figure 3.** Electrochemical test of all samples: a) LSV curves, b) Tafel slopes. c) Comparison of  $h_{10}$  values (potentials required to reach  $10 \text{ mA cm}^{-2}$  and Tafel slopes for all catalysts. d) Nyquist plots at  $10 \text{ mA cm}^{-2}$ .

not the C-30s (Figure S8, Supporting Information). This indicates that the carbon shell effectively protects the active materials from dissolution in KOH solution.

Finally, to further demonstrate the versatility of our fabrication strategy, we also used C-plasma to treat  $\text{Co}_3\text{O}_4$  nanowire arrays (data presented in Figure S9, Supporting Information).

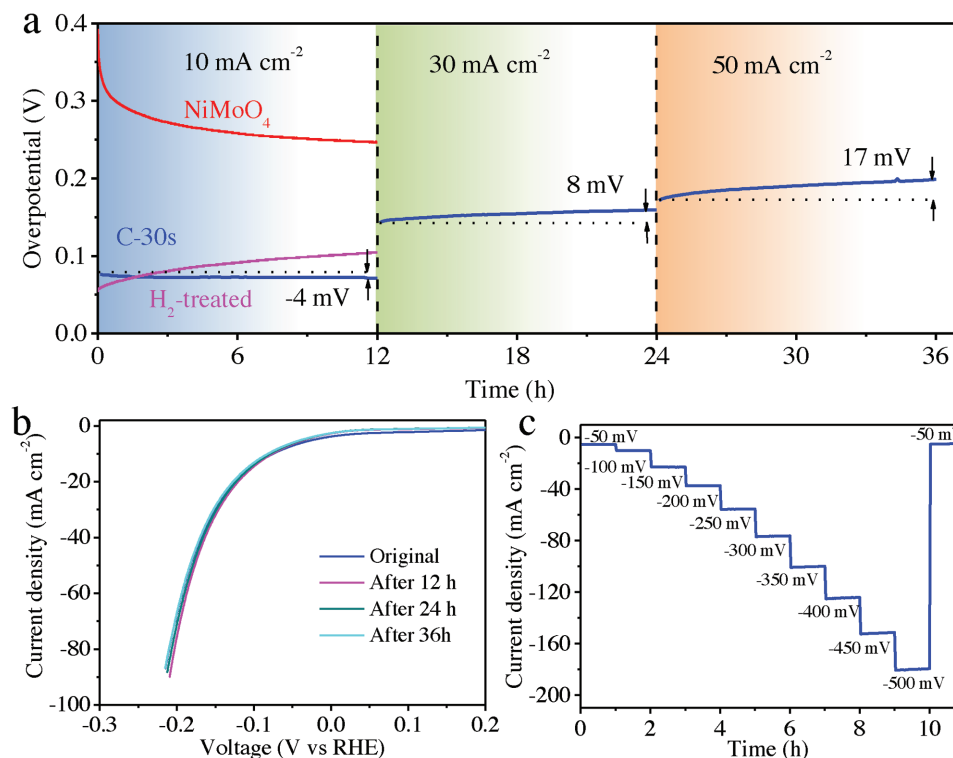


**Figure 4.** Stability test. a) Pristine  $\text{NiMoO}_4$  nanowire, and C-30s sample, as well as another sample after  $\text{H}_2$  treatment. b) LSV curves of the C-30s electrode under different HER test stage. c) C-30s at different overpotentials (without iR-correction).

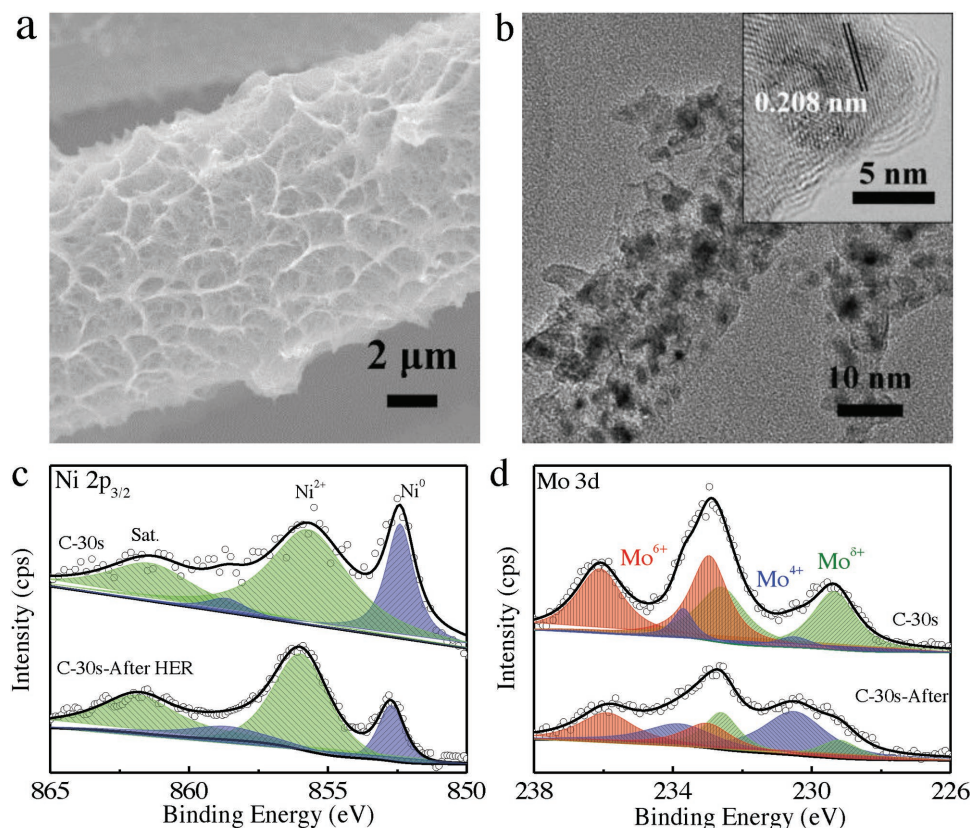


**Figure 5.** C-30s sample after stability test. a) SEM, b) TEM, c) Ni  $2p_{3/2}$  XPS spectra, and d) Mo 3d XPS spectra.

After the C-plasma treatment, the nanowire morphology was retained and lower valence CoO phase was generated. Similarly, a thin layer of graphitic carbon shell formed on the CoO nanowire surface. Compared with  $H_2$  annealing, the prereduction of  $Co_3O_4$  via C-plasma treatment not only improve the HER catalytic activity but also the longtime stability.

In summary, we have demonstrated that prereduction of transition metal oxides is an efficient method to greatly improve their catalytic activity for hydrogen evolution. Compared with the common  $H_2$  annealing, the C-plasma treatment not only has a reduction reaction function, but also leads to a concurrent encapsulation of the whole nanowire with a thin layer of graphitic carbon. Benefiting from the protection of carbon shell, the modified metal oxide exhibits outstanding physical and chemical stability under longtime and intermittent operation for hydrogen evolution. We show that this strategy is generic and also effective to other metal oxides (such as  $Co_3O_4$ ), which paves a new way to exploit transition metal oxide materials as highly active and stable HER catalysts to compete against precious metals.

## Experimental Section

**Material Synthesis:** Nickel acetate ( $NiAc_2 \cdot 4H_2O$ , 1.24 g) and ammonium molybdate ( $(NH_4)_6Mo_7O_{24} \cdot 4H_2O$ , 1 g) were added to a mixed solution (30 mL deionized (DI) water and 30 mL ethylene glycol) under magnetic stirring to give a green solution. Then, the solution was

transferred into a Teflon-lined stainless steel autoclave liner. A piece of clean carbon cloth was immersed into the reaction solution. The liner was sealed in a stainless steel autoclave and maintained at  $140^\circ C$  for 10 h. After cooling to room temperature, samples were washed with DI water and ethanol in sequence, dried in oven at  $60^\circ C$  and then annealed in furnace at  $450^\circ C$  under Ar atmosphere for 30 min to remove moisture. The average mass was about  $1.2 \text{ mg cm}^{-2}$ . Finally, the  $NiMoO_4$  was directly subjected to C-plasma to be modified. After  $NiMoO_4$  was inserted into the reactor chamber, the temperature of chamber was increased to  $450^\circ C$  and the pressure was pumped down to 0.2 mbar. Subsequently, a feedstock of ethanol was introduced. The RF-plasma discharge was conducted at 300 W and 13.56 MHz for different treatment time, i.e., 15, 30, and 60 s and the resulting products were denoted as C-15s, C-30s, and C-60s, respectively.

For comparison, the obtained  $NiMoO_4$  was partially reduced via heating under  $H_2/Ar$  (2:98) atmosphere at  $450^\circ C$  for 1 h with 100 sccm.

$Co_3O_4$  nanowire arrays grown on Ni foam were fabricated as previous report.<sup>[21]</sup> And the plasma parameters are the same as that for  $NiMoO_4$  and the treatment time was 30 s.

**Sample Characterization:** The morphology and phase of samples were characterized by field emission SEM (FEI SIRION), XRD (6000 Shimadzu), high-resolution transmission electron microscopy (FEI Tecnai G2 20), and XPS (Thermo Fisher Scientific Theta Probe).

**Electrochemical Characterization:** All electrochemical measurements were performed on an electrochemical workstation (Zahner zennium, Germany) in a glass cell with a three-electrode setup. The samples were used as the working electrode; carbon rod ( $D = 8 \text{ mm}$ ) and  $Ag/AgCl$  (3 M KCl) were used as the counter electrode and reference electrode, respectively. 1 M KOH solution ( $pH = 13.6$ ) was used as the electrolyte. All potential were calculated with respect to reversible hydrogen electrode (RHE) via the following equation:  $E(RHE) = E(Ag/AgCl) + 0.059 \text{ pH} + 0.210 \text{ V}$ . All samples were first conducted the cyclic voltammetry test to

get a stable curve at 50 mV s<sup>-1</sup>. LSV and chronoamperometric tests were conducted to evaluate the HER catalytic activity of the samples. The LSV tests were carried out at a scan rate of 5 mV s<sup>-1</sup>. The Tafel plots were derived from LSV curves which were tested at the scan rate of 1 mV s<sup>-1</sup>. The EIS were conducted at the current density of 10 mA cm<sup>-2</sup>, in a frequency from 100 kHz to 50 mHz with an AC amplitude of 5 mV.

## Supporting Information

Supporting Information is available from the Wiley Online Library or from the author.

## Acknowledgements

Y.Q.Z. and B.O. contributed equally to this work. This work was supported by the National Natural Science Foundation of China (Grant No. 51728204). It was also supported by the Singapore MOE AcRF Tier 1 grant (RG98/15) and Tier 2 grant (MOE2017-T2-1-073). The authors thank Qiaobao Zhang for the STEM image and EDS elemental mapping measurement (Xiamen University).

## Conflict of Interest

The authors declare no conflict of interest.

## Keywords

carbon shells, electrocatalysis, hydrogen evolution reaction, metal oxide, plasma treatment

Received: January 25, 2018  
Revised: March 4, 2018  
Published online:

- [1] M. A. Pellow, C. J. M. Emmott, C. J. Barnhart, S. M. Benson, *Energy Environ. Sci.* **2015**, *8*, 1938.
- [2] Y. Jiao, Y. Zheng, M. Jaroniec, S. Z. Qiao, *Chem. Soc. Rev.* **2015**, *44*, 2060.
- [3] C. G. Morales-Guio, L.-A. Stern, X. Hu, *Chem. Soc. Rev.* **2014**, *43*, 6555.
- [4] J. Wang, H. Zhang, X. Wang, *Small Methods* **2017**, *1*, 1700118.
- [5] F. Tao, *Angew. Chem., Int. Ed.* **2016**, *55*, 15212.
- [6] X. Wang, X. Gan, T. Hu, K. Fujisawa, Y. Lei, Z. Lin, B. Xu, Z.-H. Huang, F. Kang, M. Terrones, R. Lv, *Adv. Mater.* **2016**, *19*, 1603617.
- [7] Y. Wang, Y. Zhang, Z. Liu, C. Xie, S. Feng, D. Liu, M. Shao, S. Wang, *Angew. Chem., Int. Ed.* **2017**, *56*, 5867.
- [8] Y. Zhang, B. Ouyang, J. Xu, S. Chen, R. S. Rawat, H. J. Fan, *Adv. Energy Mater.* **2016**, *6*, 1600221.
- [9] B. Cao, G. M. Veith, J. C. Neuefeind, R. R. Adzic, P. G. Khalifah, *J. Am. Chem. Soc.* **2013**, *135*, 19186.
- [10] Y.-Y. Chen, Y. Zhang, W.-J. Jiang, X. Zhang, Z. Dai, L.-J. Wan, J.-S. Hu, *ACS Nano* **2016**, *10*, 8851.
- [11] H. Ang, H. Wang, B. Li, Y. Zong, X. Wang, Q. Yan, *Small* **2016**, *12*, 2859.
- [12] H. Li, C. Tsai, A. L. Koh, L. Cai, A. W. Contryman, A. H. Fragapane, J. Zhao, H. S. Han, H. C. Manoharan, F. Abild-Pedersen, *Nat. Mater.* **2016**, *15*, 48.
- [13] Q. Ji, Y. Zhang, J. Shi, J. Sun, Y. Zhang, Z. Liu, *Adv. Mater.* **2016**, *28*, 6207.
- [14] Y.-R. An, X.-L. Fan, Z.-F. Luo, W.-M. Lau, *Nano Lett.* **2017**, *17*, 368.
- [15] Y. Tan, H. Wang, P. Liu, C. Cheng, F. Zhu, A. Hirata, M. Chen, *Adv. Mater.* **2016**, *28*, 2951.
- [16] J. Tian, Q. Liu, A. M. Asiri, X. Sun, *J. Am. Chem. Soc.* **2014**, *136*, 7587.
- [17] H. Liang, A. N. Gandhi, D. H. Anjum, X. Wang, U. Schwingenschlög, H. N. Alshareef, *Nano Lett.* **2016**, *16*, 7718.
- [18] X. Xia, Y. Zhang, D. Chao, C. Guan, Y. Zhang, L. Li, X. Ge, I. M. Bacho, J. Tu, H. J. Fan, *Nanoscale* **2014**, *6*, 5008.
- [19] J. Swaminathan, R. Subbiah, V. Singaram, *ACS Catal.* **2016**, *6*, 2222.
- [20] Y. H. Li, P. F. Liu, L. F. Pan, H. F. Wang, Z. Z. Yang, L. R. Zheng, P. Hu, H. J. Zhao, L. Gu, H. G. Yang, *Nat. Commun.* **2015**, *6*, 8064.
- [21] Y. Zhang, B. Ouyang, J. Xu, G. Jia, S. Chen, R. S. Rawat, H. J. Fan, *Angew. Chem., Int. Ed.* **2016**, *55*, 8670.
- [22] K. Xu, H. Ding, H. Lv, S. Tao, P. Chen, X. Wu, W. Chu, C. Wu, Y. Xie, *ACS Catal.* **2017**, *7*, 310.
- [23] J. Zhang, T. Wang, P. Liu, Z. Liao, S. Liu, X. Zhuang, M. Chen, E. Zschech, X. Feng, *Nat. Commun.* **2017**, *8*, 15437.
- [24] Y.-Y. Chen, Y. Zhang, X. Zhang, T. Tang, H. Luo, S. Niu, Z.-H. Dai, L.-J. Wan, J.-S. Hu, *Adv. Mater.* **2017**, *29*, 1703311.
- [25] Y. Zhang, R. S. Rawat, H. J. Fan, *Small Methods* **2017**, *1*, 1700164.
- [26] L. Xu, Q. Jiang, Z. Xiao, X. Li, J. Huo, S. Wang, L. Dai, *Angew. Chem., Int. Ed.* **2016**, *55*, 5277.
- [27] S. Dou, C. L. Dong, Z. Hu, Y. C. Huang, J. I. Chen, L. Tao, D. Yan, D. Chen, S. Shen, S. Chou, *Adv. Funct. Mater.* **2017**, *27*, 1702546.
- [28] Z. Xiao, Y. Wang, Y.-C. Huang, Z. Wei, C.-L. Dong, J. Ma, S. Shen, Y. Li, S. Wang, *Energy Environ. Sci.* **2017**, *10*, 2563.
- [29] H. Liang, H. N. Alshareef, *Small Methods* **2017**, *1*, 1700111.
- [30] L. Tao, X. Duan, C. Wang, X. Duan, S. Wang, *Chem. Commun.* **2015**, *51*, 7470.
- [31] L. M. Madeira, M. F. Portela, C. Mazzocchi, A. Kaddouri, R. Anouchinsky, *Catal. Today* **1998**, *40*, 229.
- [32] M. Gong, W. Zhou, M.-C. Tsai, J. Zhou, M. Guan, M.-C. Lin, B. Zhang, Y. Hu, D.-Y. Wang, J. Yang, S. J. Pennycook, B.-J. Hwang, H. Dai, *Nat. Commun.* **2014**, *5*, 4695.
- [33] P. Reyes, I. Concha, G. Pecchi, J. L. G. Fierro, *J. Mol. Catal. A: Chem.* **1998**, *129*, 269.
- [34] H. Lin, Z. Shi, S. He, X. Yu, S. Wang, Q. Gao, Y. Tang, *Chem. Sci.* **2016**, *7*, 3399.